# Molecular Dynamics of Spider Dragline Silk Fiber Investigated by $^2$H MAS NMR

Xiangyan Shi,[†] Gregory P. Holland,*[,‡] and Jeffery L. Yarger*[,§]

[†]Department of Chemistry, University of Illinois at Urbana−Champaign, 600 South Mathews Avenue, Urbana, Illinois 61801, United States

[‡]Department of Chemistry and Biochemistry, San Diego State University, 5500 Campanile Drive, San Diego, California 92182-1030, United States

[§]Department of Chemistry and Biochemistry, Magnetic Resonance Research Center, Arizona State University, Tempe, Arizona 85287-1604, United States

Ⓢ *Supporting Information*

**ABSTRACT:** The molecular dynamics of the proteins that comprise spider dragline silk were investigated with solid-state $^2$H magic angle spinning (MAS) NMR line shape and spin−lattice relaxation time ($T_1$) analysis. The experiments were performed on $^2$H/$^{13}$C/$^{15}$N-enriched *N. clavipes* dragline silk fibers. The silk protein side-chain and backbone dynamics were probed for Ala-rich regions ($\beta$-sheet and $3_1$-helical domains) in both native (dry) and supercontracted (wet) spider silk. In native (dry) silk fibers, the side chains in all Ala containing regions undergo similar fast methyl rotations ($>10^9$ s$^{-1}$), while the backbone remains essentially static ($<10^2$ s$^{-1}$). When the silk is wet and supercontracted, the presence of water initiates fast side-chain and backbone motions for a fraction of the $\beta$-sheet region and $3_1$-helicies. $\beta$-Sheet subregion 1 ascribed to the poly(Ala) core exhibits slower dynamics, while $\beta$-sheet subregion 2 present in the interfacial, primarily poly(Gly-Ala) region that links the $\beta$-sheets to disordered $3_1$-helical motifs, exhibits faster motions when the silk is supercontracted. Particularly notable is the observation of microsecond backbone motions for $\beta$-sheet subregion 2 and $3_1$-helicies. It is proposed that these microsecond backbone motions lead to hydrogen-bond disruption in $\beta$-sheet subregion 2 and helps to explain the decrease in silk stiffness when the silk is wet and supercontracted. In addition, water mobilizes and softens $3_1$-helical motifs, contributing to the increased extensibility observed when the silk is in a supercontracted state. The present study provides critical insight into the supercontraction mechanism and corresponding changes in mechanical properties observed for spider dragline silks.

## INTRODUCTION

Spider silk attracts scientific interest because of its unique combination of strength and extensibility that makes it one of the toughest materials known.[1−4] Two proteins, major ampullate spidroin 1 (MaSp1)[5] and 2 (MaSp2),[6] comprise dragline silk and assemble into a fiber with outstanding mechanical properties.[1−3] The secondary structure of spider dragline silk has been studied using solid-state NMR and X-ray diffraction (XRD).[7−13] The repetitive motifs, poly(Ala) and poly(Gly-Ala), constitute the $\beta$-sheet nanocrystalline domains, responsible for the strength of spider silk.[7,11,13] Gly-Pro-Gly-X-X and Gly-Gly-X motifs form type II $\beta$-turn and disordered $3_1$-helical structures, respectively, that provide the estensibility of spider silk.[7,11,13] Interaction with water causes spider dragline silk to contract up to 50% in length and swell in diameter, a process known as supercontraction.[14−17] This process is accompanied by an increase in extensibility and a decrease in stiffness, resulting in rubber-like mechanical properties.[14−17] Recently, we investigated the molecular structural and dynamical changes for Gly-Pro-Gly-X-X regions in super-contracted (wet) spider dragline silk using solid-state NMR.[12,18] Although the results help to understand the

increased extensibility observed in wet, supercontracted silk, they do not explain the decrease in stiffness. The hydrogen bonding of $\beta$-sheet regions highly correlate with the stiffness of spider dragline silk.[19−22] Previous NMR and XRD studies showed that no major secondary structural change occurs and the $\beta$-sheet nanocrystalline regions only lose orientational order with respect to the fiber axis in supercontracted dragline silk but, otherwise, remain intact.[10,23−25] Further, it was shown that the minor ampullate silk exhibits a similar reorientation in the wet state but without any appreciable contraction of the fiber.[24] Thus, the disordering of the $\beta$-sheet nanocrystalline regions cannot explain the supercontraction behavior alone. In contradiction, a Raman spectroscopy study concluded that the $\beta$-sheet content likely decreases when spider silk is supercontracted.[26] In order to understand silk supercontraction behavior at the molecular level, we present a molecular dynamic study for Ala residing regions, dominantly located in $\beta$-sheet domains, for spider dragline silk in both dry and wet states.

*N. clavipes* dragline silk was used as a representative model for orb-weaving dragline silks for dynamic study in the current work. The molecular dynamics of spider dragline silk proteins are investigated by deuterium ($^2$H) magic angle spinning (MAS) solid-state NMR. $^2$H quadrupole line shapes and spin−lattice relaxation times ($T_1$) deliver rich information about molecular motion and geometry.[27−30] A recently developed technique, two-dimensional (2D) $^2$H−$^{13}$C heteronuclear correlation (HETCOR) MAS NMR,[31] was implemented to extract site-specific $^2$H line shapes for the silk sample with multiple isotopically labeled sites. In addition, $^2$H $T_1$s were indirectly measured through a $^{13}$C-detected $^2$H−$^{13}$C cross-polarization (CP) method in a site-specific fashion.[31] The detected information together with one-dimensional (1D) $^2$H MAS NMR provides an in depth view of the silk protein backbone and side-chain dynamics for Ala-rich regions in spider silk. The results provide critical molecular insight into the mechanical property changes observed for supercontracted spider silk fibers.

## ■ MATERIALS AND METHODS

**Sample Preparation.** The isotope-labeled dragline silk was collected from adult female spiders using a method as described in previous studies.[32] The silking process was monitored under a microscope to ensure only collection of major ampullate silk and avoid contamination from minor ampullate silk. The isotope labeled silk was collected from *N. clavipes* spiders fed with 45−55 μL of a 16% (w/v) U-[$^2$H$_4$,$^{13}$C$_3$,$^{15}$N]-Ala (Cambridge Isotopes, Andover, MA) aqueous solution during each forcible silking process. The spiders were fed with crickets once a week. After NMR experiments conducted on dry silk, the sample was soaked in deuterium-depleted water for a minimum of 2 h to achieve saturation and prepare supercontracted (wet) silk for NMR measurements. Surpercontracted silk was wetted (using deuterium-depleted water) and dried (under room temperature and atmospheric pressure) for several times to ensure that exchangeable deuterons (-ND or -OD group) were completely replaced by hydrogen.

**NMR Spectroscopy.** Solid-state NMR experiments were conducted on a Varian VNMRS 400 MHz spectrometer equipped with a 3.2 mm MAS probe operating in a triple resonance mode ($^1$H/$^{13}$C/$^2$H) at room temperature (298 K). Heating effects caused by spinning leads to an actual sample temperature of 303 K (temperature was calibrated with lead nitrate[33]). $^2$H−$^{13}$C HETCOR MAS and $^{13}$C-detected $^2$H $T_1$ measurement experiments were set up as described in one of our recent publications.[31] In the $^2$H−$^{13}$C HERCOR experiments, a 91 kHz (2.75 μs π/2 pulse) $^2$H rf field was employed and ∼2 kHz $^2$H GARP decoupling was utilized during signal acquisition. The $^{13}$C and $^2$H chemical shifts were indirectly referenced to the adamantane downfield resonance at 38.56 ppm and the D$_2$O resonance at 4.788 ppm, respectively. Experiments were performed using a 10 kHz MAS frequency for both dry (native material) and wet (supercontracted) silk and have the following additional parameters.

2D $^2$H−$^{13}$C HETCOR MAS experiment: 25 kHz sweep width in $^{13}$C dimension, 500 kHz sweep width with 160 $t_1$ points in $^2$H dimension, 40.96 ms acquisition time, 1.4 ms $^2$H−$^{13}$C CP contact time, a recycle delay of 0.75 s and 1024 scans. To obtain a $^2$H−$^{13}$C chemical shift correlation spectrum with higher resolution, another 2D $^2$H−$^{13}$C HETCOR MAS NMR experiment was performed with rotor-synchronized sampling (10 kHz sweep width) and 48 $t_1$ points in $^2$H dimension.

1D $^2$H−$^{13}$C CP-MAS experiment: 25 kHz sweep width, 40.96 ms acquisition time, 1.4 ms $^2$H−$^{13}$C CP contact time, 0.75 s relaxation delay time and 4096 scans.

$^{13}$C-detected $^2$H $T_1$ measurement through $^2$H−$^{13}$C CP experiment: 25 kHz sweep width, 40.96 ms acquisition time, 1.4 ms $^2$H−$^{13}$C CP contact time, 1 s recycle delay time (3 s for supercontracted, wet silk), and 10240 scans (1664 scans for supercontracted, wet silk).

$^2$H solid-echo experiment: 500 kHz sweep width, 142.88 ms acquisition time, a recycle delay of 0.75 s, and 15360 scans. The rotor-synchronized delay between the two π/2 pulses was 100 μs. A 20 μs delay was set between the second π/2 pulse and the beginning of data acquisition. The acquired FID was left shifted by 46 points prior to Fourier transform during data processing to correct spectrum phase.

$^2$H one-pulse experiment: 500 kHz sweep width, 142.88 ms acquisition time, a recycle delay of 0.75 s and 15360 scans, and 20 μs delay between the π/2 rf pulse and the beginning of acquisition. During data processing, the raw FID was left shifted by 49 points prior to Fourier transform to eliminate spectrum phase distortion caused by transmitter ring down.

1D $^2$H liquid-state NMR spectra were collected on an Agilent Inova 500 MHz spectrometer equipped with a 5 mm Inverse Direct Broadband PFG Probe. The experiments were performed on hydrolyzed U-[$^2$H$_4$,$^{13}$C$_3$,$^{15}$N]-Ala and $^2$H$_3$-Ala labeled silk. About 1 mg of each silk sample was hydrolyzed in 6 M HCl for 2 days at 108 °C, then reconstituted in 700 μL of H$_2$O and transferred to a 5 mm NMR tube. Data was acquired using the lock channel. The pulse sequence is a π/2 deuterium excitation pulse followed by data acquisition. Additional experimental parameters include 1535.63 Hz sweep width, 2.049 ms acquisition time, and a recycle delay of 5 s.

**$^2$H NMR Quadrupole Line Shape Simulations.** The $^2$H MAS quadrupole line shape simulations were conducted using SPINE-VOLUTION 3.4.4 software packages.[34] All simulations were performed with the ASG powder orientation calculation scheme. (C$_Q$ = 160 kHz and η = 0) and (C$_Q$ = 167 kHz and η = 0) were used for methyl and methine deuterium, respectively.[35,36] For the Ala backbone motion where the entire methyl group undergoes two site reorientation, simulations were performed with various reorientation angles and rates, and compared with experimental data to find the best match.

## ■ RESULTS AND DISCUSSION

**Isotope Incorporation.** Selective $^2$H labeling is difficult or impossible to achieve for native spider silk proteins.[37] In previous studies,[10] isotope labeled silk fibers were prepared by feeding spiders with $^2$H$_3$-Ala for 1D $^2$H solid-state NMR, aiming to obtain site-specific Ala methyl deuterium quadrupole line shapes and $T_1$s. However, as shown in Figure 1, isotope-labeled silk fibers obtained using this method have deuterium enriched at the Ala and Gly $^2$Hα, that could possibly lead to
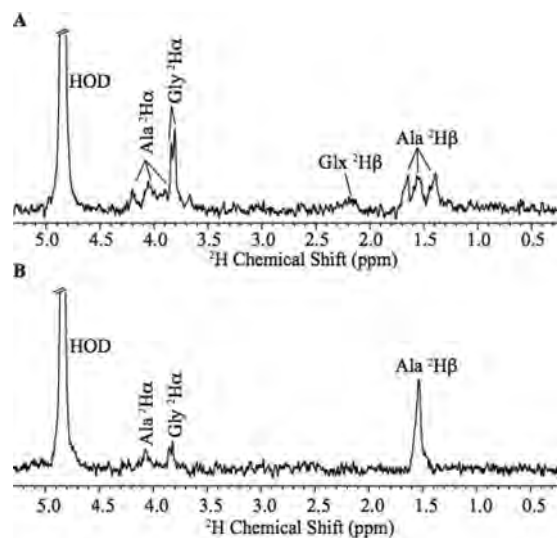


**Figure 1.** $^2$H liquid-state NMR spectra of hydrolyzed isotope labeled spider dragline silk. Silk fibers were collected from *N. clavipes* spiders fed with (A) U-[$^2$H$_4$, $^{13}$C$_3$, $^{15}$N]-Ala and (B) $^2$H$_3$-Ala aqueous solution.

misinterpreting the data in conventional 1D $^2$H NMR. The difficulty of selective labeling limits the utilization of 1D $^2$H solid-state NMR to extract correct $^2$H quadrupole patterns for a given site. This motivates the development and implementation of 2D NMR experiments such as $^2$H−$^{13}$C HETCOR for dynamic studies. In the present work, solid-state NMR measurements were performed for silk collected from *N. clavipes* spiders, where U-[$^2$H$_4$,$^{13}$C$_3$,$^{15}$N]-Ala was dissolved in their water supply. Liquid-state NMR of the hydrolyzed silk reveals that deuterium is enriched at multiple sites in the silk proteins in addition to Ala, including Gly $^2$H$\alpha$ and Glx $^2$H$\beta$ (Figure 1A). Further, the $^2$H *J*-coupling patterns indicate that $^2$H−$^{13}$C pairs selectively label the Ala residues in the silk proteins.

**$^2$H−$^{13}$C HETCOR MAS NMR and Spider Silk Protein Dynamics.** The experiments were first performed on dry spider dragline silk fibers (referring to the native material). A 2D $^2$H−$^{13}$C HETCOR experiment was conducted with rotor-synchronized sampling in $^2$H dimension to eliminate the sidebands and collect a high-resolution chemical shift correlation spectrum (Figure S1). The data illustrates the site-specific nature of the $^2$H quadrupole line shapes extracted from the 2D HETCOR MAS NMR experiments. To obtain the $^2$H quadrupole line shapes, a 2D spectrum was collected with a larger sweep width ensuring to cover the entire $^2$H MAS manifolds. The extracted site-specific Ala $^2$H$\alpha$ and $^2$H$\beta$ quadrupole line shapes are displayed in Figure 2. $^2$H quadrupole patterns correlating to the two different C$\beta$ resonances (17.4 and 20.9 ppm[7]) are identical, indicating that Ala $^2$H$\beta$ present in the $\beta$-sheet and 3$_1$-helical regions possess the same quadrupole line shapes. $^2$H quadrupole line shape
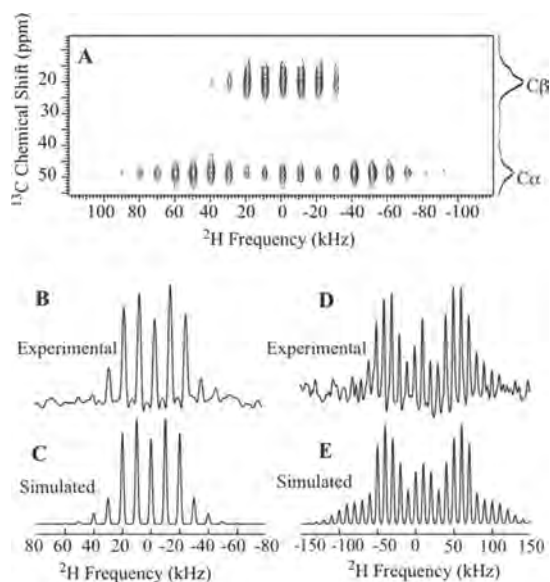


**Figure 2.** (A) $^2$H−$^{13}$C HETCOR MAS NMR spectrum for *N. clavipes* dragline silk collected from spiders fed with U-[$^2$H$_4$,$^{13}$C$_3$,$^{15}$N]-Ala aqueous solution. Rotor spinning frequency is 10 kHz. (B) Ala $^2$H$\beta$ quadrupole line shapes extracted from the 2D spectrum. (C) Simulated $^2$H quadrupole line shape for methyl deuterium undergoing three-site reorientations about the $C_{3V}$ symmetry axis in the fast motion regime (>10$^8$ s$^{-1}$). (D) Ala $^2$H$\alpha$ quadrupole line shape extracted from the 2D spectrum. (E) Simulated $^2$H quadrupole line shape for rigid (<10$^2$ s$^{-1}$) deuterium. All simulations were conducted using SPINEVOLUTION.[34]

simulations were conducted and compared with experimental data to interpret the dynamics for these regions. As shown in Figure 2B,C, the Ala methyl deuterium motion is consistent with a three-site reorientation along the $C_{3V}$ axis in the fast motion regime (>10$^8$ s$^{-1}$) as expected. In addition, the experimental Ala $^2$H$\alpha$ line shape agrees well with a static MAS pattern (Figure 2D,E), illustrating the rigidity of the local backbone environment (<10$^2$ s$^{-1}$) for Ala-rich regions in dry, native dragline silk.

When silk is wet (supercontracted), signal losses were observed for both Ala C$\alpha$ and C$\beta$ in the $^2$H−$^{13}$C CP-MAS experiments (Figure 3). No Ala C$\beta$ signal is observed for the
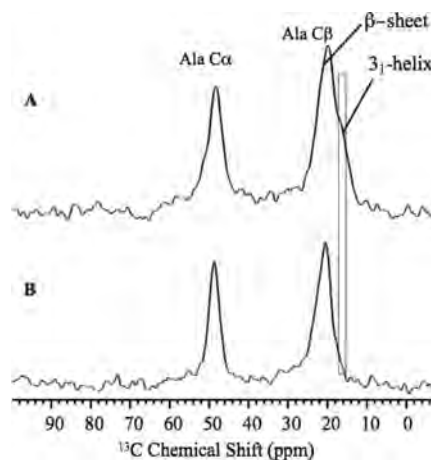


**Figure 3.** 1D $^2$H−$^{13}$C CP-MAS spectrum for (A) dry and (B) wet, supercontracted *N. clavipes* dragline silk collected from spiders fed with U-[$^2$H$_4$,$^{13}$C$_3$,$^{15}$N]-Ala aqueous solution. Two C$\beta$ chemical shifts, 20.9 and 17.4 ppm, are observed as shown in the figure, corresponding to Ala residues locate in $\beta$-sheet and 3$_1$-helical regions in silk proteins. The resonances were assigned based on previous NMR studies.[7] The two spectra were collected under the same experimental conditions and processed using the same parameters.

3$_1$-helical motifs because they become extremely mobile when in contact with water resulting in inefficient CP between $^2$H and $^{13}$C. In addition, the previously reported Ala 3$_1$-helical content is 18% for *N. clavipes* dragline silk,[13] which cannot explain the 31% C$\alpha$ and 34% C$\beta$ signal loss observed in 1D CP-MAS spectrum when the silk is wet and supercontracted. Previous NMR and XRD studies indicated that the secondary structure of the Ala-rich $\beta$-sheet region in spider dragline silk retains upon supercontraction.[10,13,23,27,38,39] Thus, there must be a CP signal loss due to Ala present in $\beta$-sheet regions that interact with water in wet silk. The 2D HETCOR NMR was also performed on the wet, supercontracted silk (Figure S2). As shown in the figure, a population of Ala residues located in $\beta$-sheet motifs in wet silk, that are rigid enough to give $^2$H−$^{13}$C CP signal, have the methyl deuterium undergoing fast three-site reorientation (>10$^8$ s$^{-1}$) and backbone remaining rigid (<10$^2$ s$^{-1}$).

**Motional Rates and the Existence of Two $\beta$-Sheet Components.** The dynamic time scale of the three-site reorientation for Ala side-chain is determined as larger than 10$^8$ s$^{-1}$, where $^2$H quadrupole line shape cannot provide the exact motional rate.[40−42] $^2$H $T_1$ is an alternative tool for exploring molecular dynamics on the 10$^8$ s$^{-1}$−10$^{12}$ s$^{-1}$ time scale.[27−29] In the present work, $^2$H $T_1$s are indirectly measured using $^{13}$C-detected $^2$H−$^{13}$C CP-MAS NMR for both dry (native) and wet

(supercontracted) silk. The inversion–recovery data was fit to extract the $^2H\beta$ $T_1$s for Ala residues present in different secondary structures in dry silk. The $^2H\beta$ relaxation data could not be fit by a single exponential function for Ala residues in $\beta$-sheet domains. Instead, a good fit is obtained by adding a second exponential (the sum of squares of fitting residues is 10 times smaller). Thus, two components (subregions) are distinguished for $\beta$-sheet motifs based on the data fit: 55% Ala possessing a $^2H\beta$ $T_1$ of 24 ms and 45% having a $T_1$ of 157 ms (Table 1). $^2H$ quadrupolar interaction is the dominant $T_1$

**Table 1. Ala $^2H\beta$ Spin-Lattice Relaxation Times for *N. clavipes* Dragline Silk Fibers[a]**

| | $\beta$-sheet | | |
| silk sample | component 1 $T_1$ (ms) | component 2 $T_1$ (ms) | $3_1$-helical $T_1$ (ms) |
| --- | --- | --- | --- |
| dry, native | 24 | 157 | 35 |
| wet, supercontracted | 38 | 569 | – |

[a]The values are extracted from fits of $^2H$ relaxation data (Figures S3 and S4).

relaxation mechanism and has been hypothesized as the only relevant relaxation resource when investigating dynamics for various systems.[10,43−45] When only this contribution to $T_1$ is considered, the Ala methyl deuterium three-site reorientation rate is $3 \times 10^9$ s$^{-1}$ and $2 \times 10^{10}$ s$^{-1}$ for the two components of the $\beta$-sheet regions in spider dragline silk proteins, respectively (see Supporting Information for calculation details). $T_1$ is determined to be 35 ms for Ala $^2H\beta$ located in $3_1$-helical motifs, corresponding to a $^2H\beta$ reorientation rate of $4.5 \times 10^9$ s$^{-1}$. This Ala side-chain motional rate is larger than that of one component of $\beta$-sheet regions as expected. However, it is smaller than the Ala side-chain motion of the other $\beta$-sheet component, that likely result from a tight local side-chain packing environment in Ala-rich $3_1$-helical motifs in native dragline silk.

For wet, supercontracted silk, the $^{13}C$-detected Ala $^2H\beta$ relaxation data also show the presence of two components in Ala residing $\beta$-sheet domains. The Ala $^2H\beta$ $T_1$ for one component is 38 and 569 ms for the other (Table 1). This agrees with the existence of two different $\beta$-sheet components explored by the Ala $^2H\beta$ $T_1$ measurement for dry, native silk. According to the relation between $T_1$ and motional rate, three-site reorientation rate for Ala methyl deuterium in wet silk is determined as $5 \times 10^9$ s$^{-1}$ and $7 \times 10^{10}$ s$^{-1}$ for the two components, respectively. Based on the $T_1$ data fit, the weight for the two components is 84% and 16%, respectively (Figure S4). Comparing with dry silk, a lower percentage was found for the component possessing a longer $T_1$ (higher Ala $^2H\beta$ reorientation rate) in wet, supercontracted silk. This can be explained by this component exhibiting a lower CP efficiency due to the existence of additional mobility when silk proteins interact with water compared to the other component. It is indeed a result of the local backbone motion, as discussed in the following paragraph. This leads to the underestimated content for this component (16%) in wet silk fibers. Thus, the ratio of Ala residues residing in the two components of the $\beta$-sheet domains is 55:45 based on $T_1$s measured for dry silk. In addition, due to the nondetectable CP signal, $^2H$ $T_1$ is not determined for Ala residues present in $3_1$-helical regions for wet silk.

**Microsecond Backbone Dynamics Observed in Super-contracted Silk.** 1D $^2H$ solid-echo and one-pulse NMR experiments were conducted for the dragline silk in both dry and wet states. Comparing with the dry silk, a significantly decreased signal was observed for the wet silk (Figure 4A). The center peak does not show signal increase in the spectrum of wet silk, ruling out the possibility that the signal decrease was caused by the deuterons becoming isotropic. Further, for wet silk, the $^2H$ center and $\pm 1/2$ spinning sideband peaks clearly exhibit much broader line width, especially at $\leq 10\%$ peak height (Figure 4A). For example, the center peak shows a line width at 5% peak height that is three times as large as that of dry silk (Figure 4A). This indicates the existence of a $^2H$ quadrupole pattern having broad peak widths in wetted silk. It is noted that the possibility of the heterogeneity across the wet silk sample in the NMR rotor causing $^2H$ signal loss and line broadening is ruled out by several control experiments (Figures S5 and S6).

In order to extract all $^2H$ components, a peak fitting routine was implemented for 1D $^2H$ spectrum of both dry (Figure 4B) and wet silk (Figure 4C). A motionally averaged $^2H$ quadrupole line shape and a rigid $^2H$ pattern were extracted from the fits. Based on the 1D liquid-state $^2H$ NMR and 2D HETCOR experiments, the motionally averaged $^2H$ line shape should be assigned to Ala H$\beta$ and the rigid $^2H$ pattern to Ala H$\alpha$, Gly H$\alpha$, and Glx H$\alpha/\beta$. Compared with dry silk, 50% signal (integral) loss is observed for the wet silk in $^2H$ solid-echo experiments for the extracted Ala $^2H\beta$ component that possesses the classical fast three-site reorientation methyl deuterium pattern (Figure 4B1,C1). The signal loss for this component is 55% in a one-pulse experiment. In addition, fitting residuals of $^2H$ spectra indicate the presence of positive broad peaks for supercontracted (wet) silk (Figure 4C3). This differs from the case of dry silk, where fitting residuals have intensities close to zero with several outlier points caused by an imperfectly phased experimental spectrum (Figure 4B−D). Thus, the decreased Ala $^2H\beta$ signal could be explained by the molecular dynamic changes for a portion of the deuterons when silk proteins interact with water. The corresponding molecular dynamics leads to a $^2H$ MAS quadrupole pattern consisting of much broader peaks and a significantly reduced $^2H$ spin−spin relaxation time ($T_2$). The peak line width of the $^2H$ MAS quadrupole pattern is 1.2 kHz according to the fitting residual shown in Figure 4C3. $^2H$ line shape simulation suggests that such a broad $^2H$ quadrupole pattern could only be a consequence of motion on the microsecond time scale ($10^6$ s$^{-1}$). The motional rate is comparable to the $^2H$ quadrupolar interaction and leads to $^2H$ $T_2$ reaching a minimum.[47] Thus, the corresponding Ala methyl deuterium in the supercontracted dragline silk must include an additional microsecond molecular motion in addition to the fast three-site methyl reorientation. Here, a simple model is used to represent this motion, where the entire methyl group reorients between two sites separated by $80 \pm 10°$ along an external axis (Figure 4E). Considering Ala contains no additional bond on the side-chain to serve as a reorientation axis for the methyl group, the reorientation axis must be the local backbone axis. Therefore, this microsecond motion is the local backbone reorienting along its long axis. Overall, this can be simulated by the local backbone undergoing anisotropic reorientation at two sites separated by $80 \pm 10°$ along its long axis with a rate of $1 \times 10^6$ s$^{-1}$ (Figure 4E). Similar anisotropic motion about the long axis of the molecule was previously observed in other biopolymers like collagen fibrils.[29]
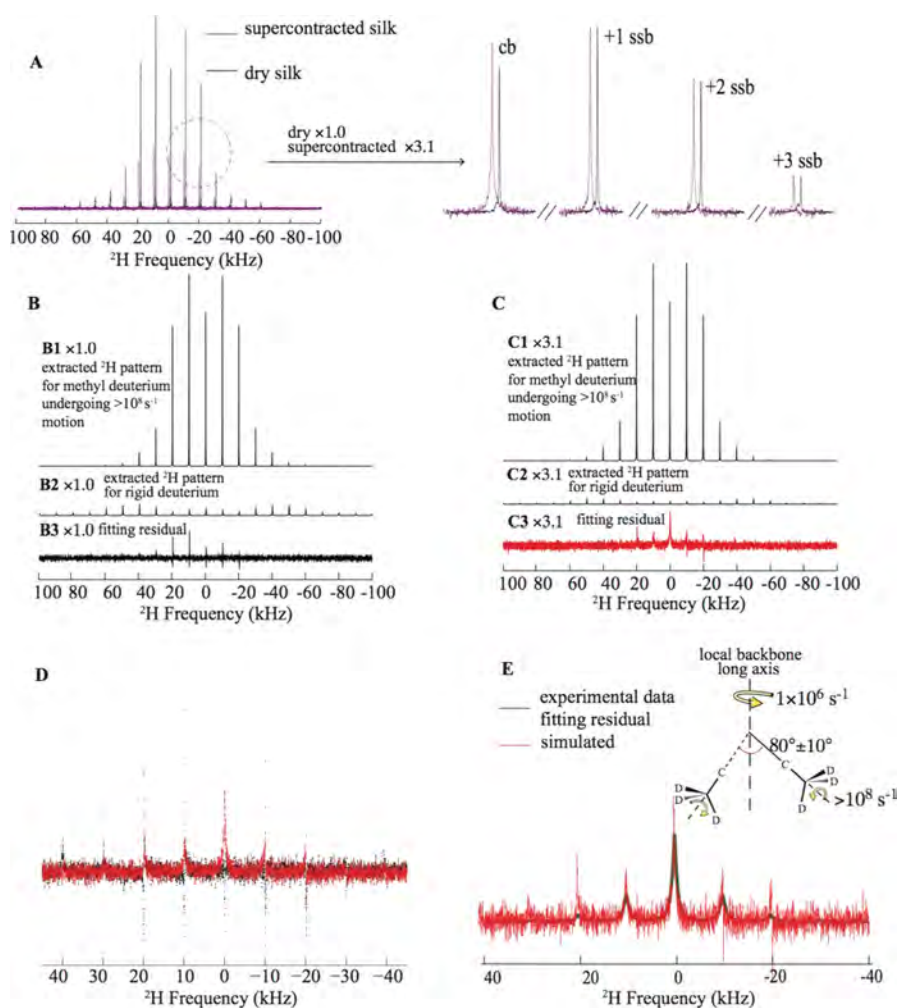
**Figure 4.** (A) $^2$H solid-echo MAS spectra for *N. clavipes* dragline silk collected from spiders fed with U-[$^2$H$_4$,$^{13}$C$_3$,$^{15}$N]-Ala aqueous solution. Centerband (cb) and +1/2/3 spinning sidebands (ssb) are expanded and shown on the right for comparison. The spectrum of supercontracted silk is slightly shifted to the right in the figure for better visualization. $^2$H solid-echo spectrum fit for (B) dry and (C) supercontracted silk. Peak fitting was performed using DMFit.[46] (D) Stacked line scatter plot of the fitting residuals for dry (black) and supercontracted (red) silk. Same vertical scale was used for the two spectra. (E) Experimental (red) and simulated (green) Ala $^2$H$\beta$ line shapes. The experimental data is the fitting residual of supercontracted silk shown in (C) and (D). Simulation was performed for methyl groups with a particular molecular motion: the entire methyl group undergoing reorientation between two sites at an angle $\theta$ with a rate $k$, while each deuterium undergoes fast three-site reorientation about the $C_{3V}$ symmetry axis. The simulated spectrum shown in the figure is obtained with $\theta = 80 \pm 10°$ and $k = 1 \times 10^6$ s$^{-1}$. The schematic representation for the motion is displayed on the upper right. Simulations are conducted using SPINEVOLUTION.[34]

**Table 2. Protein Local Backbone and Side-Chain Dynamics for Ala-Rich Regions in *N. clavipes* Dragline Silk Fibers**

| | | $\beta$-sheet subregion 1 | $\beta$-sheet subregion 2 | $3_1$-helical region |
|---|---|---|---|---|
| Ala percentage[a] | | 45−50% | 37−40% | 10−18% |
| dry, native | backbone | <10$^2$ s$^{-1}$ | <10$^2$ s$^{-1}$ | <10$^2$ s$^{-1}$ |
| | side chain | 3 × 10$^9$ s$^{-1}$ | 2 × 10$^{10}$ s$^{-1}$ | 4.5 × 10$^9$ s$^{-1}$ |
| wet, supercontracted | backbone | <10$^2$ s$^{-1}$ | 1 × 10$^6$ s$^{-1}$ | 1 × 10$^6$ s$^{-1}$ |
| | side chain | 5 × 10$^9$ s$^{-1}$ | 7 × 10$^{10}$ s$^{-1}$ | >4.5 × 10$^9$ s$^{-1}$ |

$^a$The percentage out of the total Ala residues in silk fiber.

Here, according to the signal loss observed for the three-site reorientating $^2$H$\beta$ pattern, Ala residues possessing such microsecond backbone motion account for 50−55%. This type of Ala is likely located in two different domains: $3_1$-helical motifs and partial $\beta$-sheet regions. The $\beta$-sheet region portion should be one of the two components identified by the $T_1$ measurements as discussed above.

**Full View of Protein Dynamics for Spider Dragline Silk.** As discussed above, two types of motifs are distinguished with different molecular dynamics for $\beta$-sheet domains in spider dragline silk proteins. Here, we use $\beta$-sheet subregion 1 and 2 to refer to the domains with slower and faster molecular motions, respectively. Based on the $^2$H $T_1$ measurement, as discussed above, the ratio between $\beta$-sheet subregion 1 and 2 is 55:45. Further, 1D $^2$H signal loss observed for supercontracted silk indicates that the sum of Ala residues residing in $\beta$-sheet subregion 2 and $3_1$-helical motifs accounts for 50−55%. Considering Ala residues are only present in $\beta$-sheet and $3_1$-
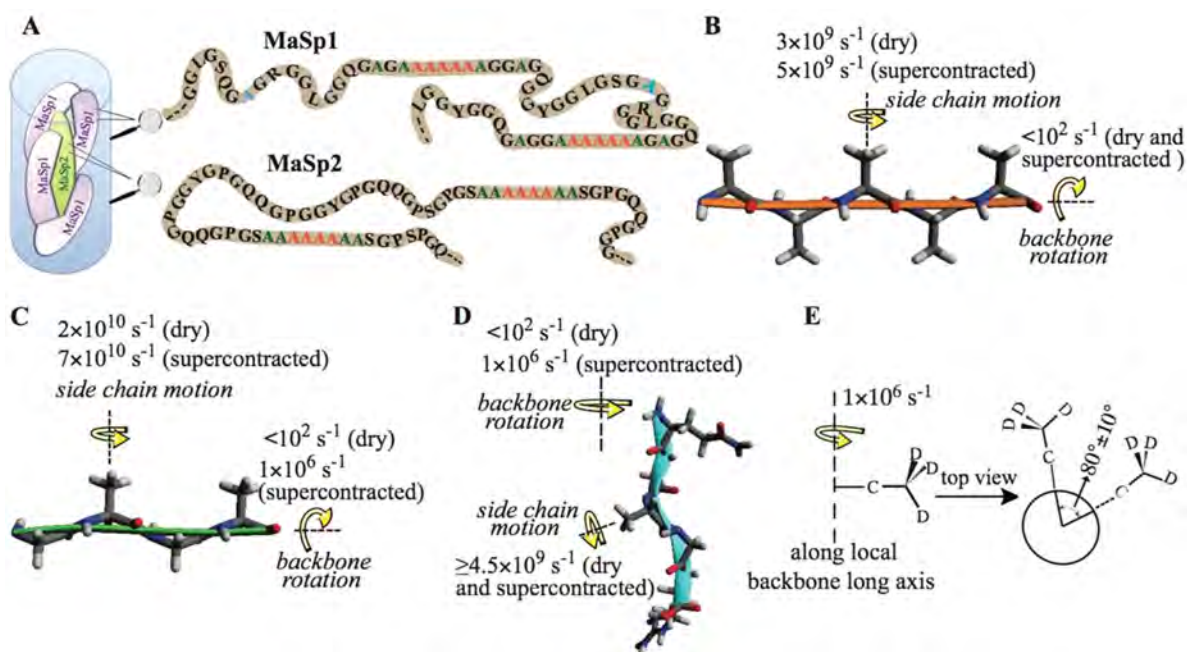
**Figure 5.** Proposed protein local backbone and side-chain dynamics for *N. clavipes* dragline silk. (A) Primary amino acid sequences for MaSp1 and MaSp2 repetitive motifs. Ala residues are highlighted for $\beta$-sheet subregion 1 (orange), $\beta$-sheet subregion 2 (green), and $3_1$-helical region (cyan). (B) Molecular dynamics model for $\beta$-sheet subregion 1. (C) Molecular dynamics model for $\beta$-sheet subregion 2. (D) Molecular dynamics model for $3_1$-helical region. (E) The side view and top view (looking down the backbone direction) of the backbone rotation for $\beta$-sheet subregion 2 and $3_1$-helical region in wet (supercontracted) silk, as shown in (C) and (D). It is the rotation along the local backbone long axis and represented by an anisotropic reorientation between two sites separated by $80 \pm 10°$ with a rate of $10^{-6}$ s$^{-1}$. The side-chain motion is Ala methyl deuterium undergoing three-site reorientations along the $C_{3V}$ symmetry axis.

helical structures in silk protein repetitive domains, the percentage of Ala in $\beta$-sheet subregion 1, 2 and $3_1$-helical regions is 45−50%, 37−40%, and 10−18%, respectively (see Supporting Information for calculation details). As discussed above, the local backbone and side-chain motional time scale was determined with $^2$H MAS NMR for the three Ala-rich regions of the silk proteins. Table 2 lists the summarized molecular dynamics for *N. clavipes* dragline silk. It illustrates that water accesses 50−55% of the Ala residues ($\beta$-sheet subregion 2 and $3_1$-helical motifs) and influence their dynamics in supercontracted dragline silk. This agrees well with previous deuterium exchange study where 50% Ala in *N. clavipes* dragline silk were found to be permeable to water.[48]

Previous solid-state NMR studies of spider dragline silk showed that poly(Ala) and poly(Gly-Ala) form $\beta$-sheet structures.[7−13] It is noted from the MaSp1 primary sequence that poly(Gly-Ala) motifs are located between poly(Ala) and the disordered helical domains.[5] This specific interfacial position makes the poly(Gly-Ala) motifs undergo faster motion compared to the poly-Ala $\beta$-sheet core domains. Thus, it is logical to assign poly(Gly-Ala) and poly-Ala domains to $\beta$-sheet subregions 2 and 1 in MaSp1, respectively (Figure 5). In MaSp2, poly-Ala $\beta$-sheet crystalline regions connect with flexible type II $\beta$-turn motifs.[6−13] In this case, partial poly(Ala) motifs are located at the interfacial positions connecting the flexible regions and $\beta$-sheet core domains, and, exhibit faster molecular motions (Figure 5). Taking into account the protein primary sequences and the ratio between MaSp1 and MaSp2,[5,6,49] a molecular dynamics model is proposed for spider dragline silk fibers in both dry and wet states (Figure 5).

**Supercontrated Silk Molecular Dynamics and Mechanical Properties.** $\beta$-Sheet subregions 1 and 2 are located

in the $\beta$-sheet core domain and the interfacial position connecting the disordered helical and turn-like motifs, respectively. Thus, being impacted differently by the disordered motifs, the two regions present unique molecular dynamics. In dry (native) silk, the local backbones appear static ($<10^2$ s$^{-1}$) for all Ala residing domains. For wet (supercontracted) silk, $\beta$-sheet subregion 2 and $3_1$-helical domains exhibit microsecond local backbone reorientation because of interaction with water. Previous studies suggested that the $\beta$-sheet interchain hydrogen bonding is the dominant source of silk strength.[18−21] Although major structures remain unchanged,[7−13,22−24] the microsecond motion exhibited by $\beta$-sheet subregion 2 disrupts the interchain hydrogen bonding which could help explain the decrease in stiffness for wet, supercontracted silk. In addition, water molecules mobilize and soften the helical regions when silk is wet, contributing to the observed increase in extensibility. Overall, the present work provides a structural and dynamic explanation for the decreased stiffness and increased extensibility observed for wet, supercontracted spider dragline silk.

## ■ CONCLUSION

Previous NMR, XRD, and Raman spectroscopy studies provided substantial information for understanding the conformational structure of native and supercontracted spider silk.[7−13,26] However, the molecular origin for the changes in mechanical properties observed for supercontracted silk has remained a mystery for decades. In this article, we presented a complete dynamic study for Ala-rich motifs in spider dragline silk that provide an explanation for the variation in mechanical properties from both a structural and a dynamic perspective. Molecular dynamics extracted from $^2$H MAS NMR in conjunction with simulations for Ala-rich regions, including $\beta$-

sheet and $3_1$-helical domains, illustrated that the $\beta$-sheet region is comprised of two components, $\beta$-sheet subregions 1 and 2, that have different dynamical features. Further, it was found that $\beta$-sheet subregion 2 and $3_1$-helical domains exhibit microsecond backbone motions in wet silk that can interrupt interchain hydrogen bonding and help explain the decrease in silk fiber stiffness when the silk is in a supercontracted state. In addition, mobilized $3_1$-helical motifs likely contribute to the observed increase in extensibility for supercontracted spider silk. The $^2$H NMR dynamic study presented here sheds new light on the spider silk supercontraction mechanism and mechanical porperties, and offers useful guidance for designing spider silk-inspired materials and fibers.

## ■ ASSOCIATED CONTENT

### ⓢ Supporting Information

Rotor-synchronized $^2$H$-^{13}$C correlation MAS NMR spectrum, $^2$H$-^{13}$C HETCOR MAS NMR spectrum for wet, super-contracted *N. clavipes* dragline silk, $^{13}$C-detected Ala $^2$H$\beta$ $T_1$ inversion recovery curves for native (dry) and supercontracted (wet) *N. clavipes* dragline silk, calculating molecular motion rate using $^2$H $T_1$, supplementary figures and discussion for the homogeneity of the supercontracted (wet) silk sample, and calculation details for percentages of different regions in *N. clavipes* dragline silk fibers. This material is available free of charge via the Internet at http://pubs.acs.org.

## ■ AUTHOR INFORMATION

### Corresponding Authors
*E-mail: gholland@mail.sdsu.edu.
*E-mail: jyarger@gmail.com.

### Notes
The authors declare no competing financial interest.

## ■ REFERENCES

(1) Lazaris, A.; Arcidiacono, S.; Huang, Y.; Zhou, J. F.; Duguay, F.; Chretien, N.; Welsh, E. A.; Soares, J. W.; Karatzas, C. N. *Science* **2002**, *295*, 472−476.
(2) Lewis, R. V. *Chem. Rev.* **2006**, *106*, 3762−3774.
(3) Vollrath, F.; Knight, D. P. *Nature* **2001**, *410*, 541−548.
(4) Hu, X.; Vasanthavada, K.; Kohler, K.; McNary, S.; Moore, M. F.; Vierra, C. *Cell. Mol. Life Sci.* **2006**, *63*, 1986−1999.
(5) Xu, M.; Lewis, R. V. *Proc. Natl. Acad. Sci. U.S.A.* **1990**, *87*, 7120−7124.
(6) Hinman, M. B.; Lewis, R. V. *J. Biol. Chem.* **1992**, *267* (27), 19320−19324.
(7) Holland, G. P.; Creager, M. S.; Jenkins, J. E.; Lewis, R. V.; Yarger, J. L. *J. Am. Chem. Soc.* **2008**, *130*, 9871−9877.
(8) Asakura, T.; Suzuki, Y.; Nakazawa, Y.; Holland, G. P.; Yarger, J. L. *Soft Matter* **2013**, *9*, 11440−11450.
(9) Benmore, C. J.; Izdebski, T.; Yarger, J. L. *Phys. Rev. Lett.* **2012**, *108*, 178102.
(10) Simmons, A. H.; Michal, C. A.; Jelinski, L. W. *Science* **1996**, *271*, 84−87.
(11) van Beek, J. D.; Hess, S.; Vollrath, F.; Meier, B. H. *Proc. Natl. Acad. Sci. U.S.A.* **2002**, *99*, 10266−10271.
(12) Jenkins, J. E.; Creager, M. S.; Butler, E. B.; Lewis, R. V.; Yarger, J. L.; Holland, G. P. *Chem. Commun.* **2010**, *46*, 6714−6716.
(13) Jenkins, J. E.; Creager, M. S.; Lewis, R. V.; Holland, G. P.; Yarger, J. L. *Biomacromolecules* **2010**, *11*, 192−200.
(14) Liu, Y.; Shao, Z.; Vollrath, F. *Biomacromolecules* **2008**, *9*, 1782−1786.
(15) Liu, Y.; Sponner, A.; Porter, D.; Vollrath, F. *Biomacromolecules* **2008**, *9*, 116−121.
(16) Work, R. W. *J. Exp. Biol.* **1985**, *118*, 379−404.
(17) Gosline, J. M.; Denny, M. W.; DeMont, M. E. *Nature* **1984**, *309*, 551−552.
(18) Shi, X.; Yarger, J. L.; Holland, G. P. *Chem. Commun.* **2014**, *50*, 4856−4859.
(19) Nova, A.; Keten, S.; Pugno, N. M.; Redaelli, A.; Buehler, M. J. *Nano Lett.* **2010**, *10*, 2626−2634.
(20) Keten, S.; Xu, Z.; Ihle, B.; Buehler, M. J. *Nat. Mater.* **2010**, *9*, 359−367.
(21) Hayashi, C. Y.; Shipley, N. H.; Lewis, R. V. *Int. J. Biol. Macromol.* **1999**, *24*, 271−275.
(22) Lee, S.; Pippel, E.; Gösele, U.; Dresbach, C.; Qin, Y.; Chandran, C. V.; Bräuniger, T.; Hause, G.; Knez, M. *Science* **2009**, *324*, 488−492.
(23) Yang, Z. T.; Liivak, O.; Seidel, A.; LaVerde, G.; Zax, D. B.; Jelinski, L. W. *J. Am. Chem. Soc.* **2000**, *122*, 9019−9025.
(24) Parkhe, A. D.; Seeley, S. K.; Gardner, K.; Thompson, L.; Lewis, R. V. *J. Mol. Recognit.* **1997**, *10*, 1−6.
(25) Holland, G. P.; Lewis, R. V.; Yarger, J. L. *J. Am. Chem. Soc.* **2004**, *126*, 5867−5872.
(26) Shao, Z.; Vollrath, F.; Sirchaisit, J.; Young, R. J. *Polymer* **1994**, *40*, 2493−2500.
(27) Torchia, D. A. *Annu. Rev. Biophys. Bioeng.* **1984**, *13*, 125−144.
(28) Krushelnitsky, A.; Reichert, D. *Prog. Nucl. Magn. Reson. Spectrosc.* **2005**, *47*, 1−25.
(29) Jelinski, L. W.; Sullivan, C. E.; Torchia, D. A. *Nature* **1980**, *284*, 531−534.
(30) Asakura, T.; Minami, M.; Shimada, R.; Demura, M.; Osanai, M.; Fujito, T.; Imanari, M.; Ulrich, A. S. *Macromolecules* **1997**, *30*, 2429−2435.
(31) Shi, X.; Yarger, J. L.; Holland, G. P. *J. Magn. Reson.* **2013**, *226*, 1−12.
(32) Work, R. W.; Young, C. T. *J. Arachnol.* **1987**, *15*, 65−80.
(33) Bielecki, A.; Burum, D. P. *J. Magn. Reson.* **1995**, *116*, 215−220.
(34) Veshtort, M.; Griffin, R. G. *J. Magn. Reson.* **2006**, *178*, 248−282.
(35) Beshah, K.; Olejniczak, E. T.; Griffin, R. G. *J. Chem. Phys.* **1987**, *86*, 4730−4736.
(36) Hologne, M.; Chen, Z.; Reif, B. *J. Magn. Reson.* **2006**, *179*, 20−28.
(37) Shi, X.; Yarger, J. L.; Holland, G. P. *Anal. Bioanal. Chem.* **2013**, *405*, 3997−4008.
(38) van Beek, J. D.; Kümmerlen, J.; Vollrath, F.; Meier, B. H. *Int. J. Biol. Macromol.* **1999**, *24*, 173−178.
(39) Work, R. W.; Morosoff, N. *Text. Res. J.* **1982**, *52*, 349−356.
(40) Hologne, M.; Hirschinger, J. *Solid State Nucl. Mag.* **2004**, *26*, 1−10.
(41) Schadt, R. J.; Cain, E. J.; English, A. D. *J. Phys. Chem.* **1993**, *97*, 8387−8392.
(42) Hologne, M.; Faelber, K.; Diehl, A.; Reif, B. *J. Am. Chem. Soc.* **2005**, *127*, 11208−11209.
(43) Torchia, D. A.; Szabo, A. *J. Magn. Reson.* **1982**, *49*, 107−121.
(44) Batchelder, L. S.; Niu, C. H.; Torchia, D. A. *J. Am. Chem. Soc.* **1983**, *105*, 2228−2231.
(45) Spiess, H. W. *NMR Basic Principles and Progress*; Springer-Verlag: Berlin/Heidelberg/ New York, 1978; Vol. *15*.
(46) Massiot, D.; Fayon, F.; Capron, M.; King, I.; Le Calvé, S.; Alonso, B.; Durand, J. O.; Bujoli, B.; Gan, Z.; Hoatson, G. *Magn. Reson. Chem.* **2002**, *40*, 70−76.
(47) Schmidt-Rohr, K.; Spiess, H. W. *Multidimensional Solid-State NMR and Polymers*; Academic Press Limited: San Diego, 1994.
(48) Li, X.; Eles, P. T.; Michal, C. A. *Biomacromolecules* **2009**, *10*, 1270−1275.

(49) Brooks, A. E.; Steinkraus, H. B.; Nelson, S. R.; Lewis, R. V. *Biomacromolecules* **2005**, *6* (6), 3095−3099.